Available online at www.sciencedirect.com
ScienceDirect
Remote Sensing of Environment 105 (2006) 9–22
Remote Sensing of Environment
www.elsevier.com/locate/rse

A comparative study of NOAA–AVHRR derived drought indices using change vector analysis

Y. Bayarjargal [a], A. Karnieli [a,*], M. Bayasgalan [b], S. Khudulmur [b], C. Gandush [a,c], C.J. Tucker [d]

[a] The Remote Sensing Laboratory, Jacob Blaustein Institute for Desert Research, Ben Gurion University of the Negev, Sede Boker Campus 84990, Israel
[b] National Remote Sensing Center, Ministry of Nature and Environment, Mongolia
[c] Institute of Meteorology and Hydrology, Ministry of Nature and Environment, Mongolia
[d] Laboratory for Terrestrial Physics, NASA/Goddard Space Flight Center, USA

Received 1 August 2005; received in revised form 26 May 2006; accepted 6 June 2006

Abstract

The objective of this study was to compare the spatial occurrences of droughts, detected by remotely sensed drought-indices over the desert-steppe and desert geo-botanical zones of Mongolia. All indices were derived from reflectance and thermal data sets, obtained from the NOAA–AVHRR data between 1982 and 1999. One group of the drought-indices is based on vegetation state derived from the reflective channels. This group includes the Normalized Difference Vegetation Index (NDVI), Anomaly of Normalized Difference Vegetation Index (NDVIA), Standardized Vegetation Index (SVI), and Vegetation Condition Index (VCI). Another group, based on surface brightness temperature derived from the thermal channel of NOAA–AVHRR, includes the Temperature Condition Index (TCI). The third group is based on combination between the reflective and thermal channels includes the ratio between Land Surface Temperature (LST) and NDVI (LST/NDVI), the Vegetation Health Index (VH), and the Drought Severity Index (DSI). Change detection procedure was performed by using the Change Vector Analysis in the temporal domain. Comparison analysis among the drought-indices reveals that there is no spatial coincidence between them, even when the vegetation growing period was divided into 2-month sub-periods — beginning, middle, and end. Based on the statistical analysis, higher correlations were found among the reflective indices while lesser or no relationships were found between the thermal and combination of the thermal and reflective indices. Furthermore, no agreement was found between the spatial extent of the satellite-derived drought-indices and the meteorological-based Palmer Drought Severity Index (PDSI) and also between the traditional ground-observed drought-affected-areas (DAA) maps. It was found that the combination of satellite-derived drought-indices can identify wider drought-occurred areas rather than the PDSI and the DAA maps. In summary, this study concludes that it is difficult to point out the most reliable drought index, and that the ground observations cannot provide sufficient information for validation of satellite derived drought indices.

Keywords: NOAA–AVHRR; Drought indices; Vegetation indices; Land surface temperature; Mongolia

1. Introduction

Although drought is a complex phenomenon, it has been defined specifically by the remote sensing community as a period of abnormally dry weather, which results in a change in vegetation cover (Heim, 2002; Tucker & Choudhury, 1987). Drought is a recurrent climate process occurs with uneven temporal and spatial characteristics over a broad area and over an extended period of time. Therefore, detecting drought onsets and ends and assessing its severity using satellite-derived information are becoming popular in disaster, desertification, and climate change studies. In the last decades, observations show that the frequency and intensity of droughts have increased in some parts of the world (Hulme & Kelly, 1993; McCarthy et al., 2001) including the Mongolian Gobi (Adyasuren, 1998). Regional climate warming in southern Mongolia has increased by 0.1 to 3.7 °C during last 60 years. In this region, there is also evidence that spring precipitation has decreased by 17%, while summer precipitation has increased by 11% (Natsagdorj, 2000). It is likely that these changes in temperature and precipitation can intensify the occurrences of drought, especially during the vegetation green-up onset

* Corresponding author. Tel.: +972 8 6596855; fax: +972 8 6596805.
E-mail address: karnieli@bgu.ac.il (A. Karnieli).

0034-4257/$ - see front matter © 2006 Elsevier Inc. All rights reserved.
doi:10.1016/j.rse.2006.06.003

time. Moreover, it was reported that the frequency of drought in the spring and summer has increased from 1–2 to 3–4 times every 5 years in the Gobi region (Bolortsetseg, Bayasgalan, Dorj, Natsagdorj, & Tuvaansuren, 2000). Drought has a disturbing effect not only on agricultural productivity and hydrological resources but also on the natural vegetation, and hence it may accelerate desertification processes when associated with destructive human activities (i.e., overgrazing) in semi-arid pastureland areas of Mongolia.

Traditionally, information on drought-affected-areas (DAA) for a certain year at a local administrative level (Soum) is derived from summertime weather observation in terms of agro-meteorological parameters (such as pasture yield, air temperature, and precipitation). Weather was categorized as favorable conditions, semi-drought, and drought, in connection with suitability for livestock grazing. Such descriptive information has been archived only in tabular, rather than cartographic, form at the Meteorological Institute of Mongolia. The DAA indicates if a drought event was observed but it does not provide any information on vegetation phenology or drought intensity on spatial and temporal domains.

With regard to the above drought definition, changes in vegetation cover detected by remote sensing in the temporal and spatial domains have been using as indicator of droughts. As integrated pressure of a deficiency of precipitation over a certain period and other climatic factors such as high temperature, high wind, and low relative humidity in particular area, droughts generally result in reduced green vegetation cover. Even though drought has a specific duration (e.g., weeks, months, years) and has decreasing results in soil moisture and vegetation growth, it ends whenever a region receives precipitation. When drought stops, reduced vegetation cover caused by the drought might recover (Nicholson et al., 1998; Prince et al., 1998) although this process occurs over time (Diouf & Lambin, 2001). In this context, the aim of the remote sensing change detection process is to measure the degree or cumulative impact of drought-related changes on the vegetation cover over time. Although a variety of change detection techniques, using remotely sensed data, have been formulated and frequently reviewed in the literature (e.g., Lunetta & Elvidge, 1998; Singh, 1989), selection of the most appropriate method for studying vegetation cover changes caused by droughts is challenging. This is because different types of change due to droughts can occur concurrently and may be interpreted in different ways. Change Vector Analysis (CVA) is a powerful change detection algorithm (Cohen & Fiorella, 1998) and can be used to detect vegetation cover changes with respect to droughts in long-term data analysis. Although CVA was developed for two spectral bands of Landsat MSS data (Kauth & Thomas, 1976), it is applicable either to any number of spectral bands or to any amount of temporal data. Virag and Colwell (1987) conceptually extended the procedure of CVA into *N*-dimensional space by using a multispectral positive and negative "sector code" accounting system, since calculation of angles of change vectors in many-dimensional space is often desirable to implement some type of simplification. By this accounting system, in each of the *N*-dimensions, the spectral change vector can get either a positive or negative code on 2N directions (Virag & Colwell, 1987). Johnson and Kasischke (1998) provided good examples of how to use the "sector code" system and how it relates to the change magnitude in change image composition. While CVA was introduced nearly two decades ago, this method has been frequently using for forest change and general land use changes (Cohen & Fiorella, 1998; Collins & Woodcock, 1996; Malila, 1980). An extension of CVA on time series observations has been used to monitor land use changes in West Africa (Lambin & Strahler 1994a). Degree and duration of drought events can be characterized by CVA as variations in magnitude and direction of the vector of vegetation cover over successive periods (Lambin & Ehrlich, 1997; Lambin & Strahler, 1994a,b).

Among other applications related to vegetation studies, numerous researchers investigated the possibility of assessing and monitoring droughts (e.g., McVicar & Jupp, 1998) using either reflective or combined responses of reflective and thermal data derived from the Advanced Very High Resolution Radiometer (AVHRR) onboard the National Oceanic and Atmospheric Administration (NOAA) satellites. The NOAA–AVHRR is the most widely applied spaceborne sensor for investigating droughts. The sensor has been orbiting the globe since the late 1970s with five spectral channels, one in the visible, one in the near infrared, one in the mid-infrared, and two in the thermal range. The sensor's data (1981–2001) is archived, maintained, and distributed by NASA (http://daac.gsfc.nasa.gov/landbio/). Its land products, Normalized Difference Vegetation Index (NDVI) and brightness temperatures, are widely used. The NDVI (Table 1) is based on the difference between the maximum absorption of radiation in the red spectral region (due to the chlorophyll pigments) and the maximum reflectance in the near infrared spectral region (due to the leaf cellular structure), and the fact that soil spectra, lacking these mechanisms, typically do not show such dramatic spectral difference (Tucker, 1979). Many studies show that NDVI can be a useful index for studying vegetation and ecosystems in semi-arid environments where vegetation cover is less than 30% (Huete & Tucker, 1991; Karnieli et al., 1996). Significant relationships between time series of NDVI and various vegetation indicators including green Leaf Area Index (LAI), green biomass production, as well as rainfall or soil moisture in semi-arid environments have been reported (Hielkema et al., 1986; Maselli et al., 1993; Nicholson & Farrar, 1994; Peters & Eve, 1995; Richard & Poccard, 1998; Schmidt & Karnieli, 2000; Tucker et al., 1985). Consequently, NOAA–AVHRR derived NDVI and other related indices (e.g., NDVI anomaly, integrated or standardized NDVI, Global Vegetation Index, Vegetation Condition Index, etc.) have been successfully used to identify and monitor areas affected by drought at regional and local scales (Gonzalez-Alonso et al., 1995, 2000; Ji & Peters, 2003; Liu & Negron-Juarez, 2001; Malingreau, 1986; Nicholson et al., 1998; Peters et al., 1993; Salinas-Zavala et al., 2002; Srivastava et al., 1997; Tucker, 1989; Tucker & Choudhury, 1987).

Tucker and Choudhury (1987) found that NDVI could be used as a response variable to identify and quantify drought disturbance in semi-arid and arid lands since its low values correspond to stressed vegetation. Recently, Ji and Peters (2003) found that NDVI is an effective indicator of vegetation response to drought in the Great Planes of the USA, based on the

Table 1
The NOAA–AVHRR images-derived and meteorological-measured drought-indices

Drought indices	Formula*	Source and reference
(1) Normalized Difference Vegetation Index (NDVI)	$NDVI_{ijk} = \frac{(NIR_{ijk} - R_{ijk})}{(NIR_{ijk} + R_{ijk})}$	Ji & Peters, 2003; Tucker, 1979; Tucker & Choudhury, 1987
(2) Anomaly of Normalized Difference Vegetation Index (NDVIA)	$NDVIA_{ijk} = \overline{NDVI}_{ij} - NDVI_{ijk}$	Anyamba et al., 2001
(3) Standardized Vegetation Index (SVI)	$SVI_{ijk} = \frac{(NDVI_{ijk} - \overline{NDVI}_{ij})}{\sigma NDVI_{ij}}$	Liu & Negron-Juarez, 2001; Peters et al., 2002
(4) Vegetation Condition Index (VCI)	$VCI_{ijk} \frac{(NDVI_{ijk} - NDVI_{i,\min})}{(NDVI_{i,\max} - NDVI_{i,\min})}$	Kogan, 1990, 1995, 1997, 2000
(5) Temperature Condition Index (TCI)	$TCI_{ijk} = \frac{(BT_{i,\max} - BT_{ijk})}{(BT_{i,\max} - BT_{i,\min})}$	Kogan, 1995, 1997, 2000
(6) Vegetation Health Index (VH)	$VH_{ijk} = 0.5^{*} VCI_{ijk} + 0.5^{*} TCI_{ijk}$	Kogan, 1997, 2000, Kogan et al., 2004
(7) Ratio between LST and NDVI (LST/NDVI)	$LST_{ijk}/NDVI_{ijk}$	Karnieli & Dall'Olmo, 2003; Lambin & Ehrlich, 1996; McVicar & Bierwirth, 2001
(8) Drought Severity Index (DSI)	$DSI_{ijk} = \Delta LST_{ijk} - \Delta ANDVI_{ijk}$; $\Delta LST_{ijk} = (\overline{LST}_{ij} - LST_{ijk})/\sigma LST_{ij}$ $\Delta NDVI_{ijk} = (\overline{NDVI}_{ij} - NDVI_{ijk})/\sigma NDVI_{ij}$	Bayarjargal et al., 2000
(9) Palmer Drought Severity Index (PDSI)	$PDSI_{ijk} = PDSI_{ik}\{j-1+ \left[\frac{Z_{ijk}}{3} + 0.103^{*} PDSI_{ij-1k}\right]\}$	Dai et al., 2004; Palmer, 1965; National Drought Mitigation Center, 2003

*NIR_{ijk} and R_{ijk} — reflectance values at the near-infrared (channel 2) and red (channel 1) wavelengths of NOAA–AVHRR, respectively, for pixel i during month j for year k. Note that j can be also referred to 8-day (e.g. MODIS data), 10-day (e.g. PAL AVHRR), 14-day (1 km AVHRR), 16-day (1 km MODIS), depending on the time intervals of data sets.
$NDVI_{ijk}$ — monthly NDVI for pixel i in month j for year k.
$\overline{NDVI}_{ij}$ — multiyear average NDVI for pixel i in month j.
$\sigma NDVI_{ij}$ — standard deviation of NDVI for pixel i in month j.
$NDVI_{i,\min}$ and $NDVI_{i,\max}$ — multiyear minimum and maximum NDVI, respectively, for pixel i.
BT_{ijk} — brightness temperature at channel 4 for pixel i in month j for year k.
$BT_{i,\min}$ and $BT_{i,\max}$ — multiyear minimum and maximum brightness temperature, respectively, for pixel i.
LST_{ijk} — land surface temperature for pixel i in month j for year k.
$\overline{LST}_{ij}$ — multiyear average LST for pixel i in month j.
σLST_{ij} — standard deviation of LST for pixel i in month j.
$PDSI_{ijk}$ and $PDSI_{ij-1k}$ — monthly PDSI for pixel i for year k in a current month j and previous month $j-1$.
Z_{ijk} — monthly moisture status for pixel i in month j for year k.

relationships between the NDVI and meteorological-drought index. Since NDVI has proven that it represents vegetation responses in a timely manner to climate variability as a normalized ratio, the Vegetation Condition Index (VCI, Table 1), which is NDVI normalization for each pixel based on minimum and maximum NDVI values over time, was developed by Kogan (1990, 1995) in order to relatively assess changes in the NDVI signal through time by reducing the influence of local ecosystem variables. Anyamba et al. (2001) used NDVI anomaly (NDVIA, Table 1), which is a departure of NDVI from its long-term average for a specific month, in order to indicate drought conditions as compared to the average on a range of time scales. More recently, historical drought induced by El Niño Southern Oscillation in northeast Brazil, coincided with the NDVIA when it was standardized based on its standard deviation (Liu & Negron-Juarez, 2001). In addition, the probability of the standardized NDVI anomaly, the Standardized Vegetation Index (SVI, Table 1), has been used to monitor areas affected by drought and vegetation conditions in terms of relative greenness at pixel level over time periods (Peters et al., 2002). The NDVIA and SVI have been successfully used to monitor drought conditions over Africa and America (Anyamba et al., 2001; Peters et al., 2002; http://svs.gsfc.nasa.gov/stories/drought/index.html; http://www.drought.unl.edu/dm/index.html).

Gutman (1990) showed that the thermal data from polar orbiters might be useful for detecting the inter-annual changes in surface moisture, when the change in the vegetation index fails to produce a significant signal. Several authors used a thermal and a combined responses of reflective (e.g., NDVI, VCI) and thermal (e.g., land surface temperature (LST), brightness temperature)

products of the NOAA–AVHRR to provide a more ecological and physical interpretation of remotely sensed data for examining drought conditions (Bayarjargal et al., 2000; Gutman, 1990; Karnieli, 2000; Karnieli & Dall'Olmo, 2003; Kogan, 1997, 2000; Kogan et al., 2004; McVicar & Jupp, 1998). Combined utilization of NDVI and LST (referring hereafter as hybrid indices) is based on the strong negative correlation between those two variables, due to increase in evaporation with a decrease in soil moisture, caused by higher temperature, which results in a decline of the vegetation cover, where water is the main limiting factor for vegetation growth (Karnieli et al., in press; Lambin & Ehrlich, 1996; Nemani & Running, 1989).

Kogan (1995) adapted the VCI normalization approach to include brightness temperature in the NOAA–AVHRR channel 4 and developed the Temperature Condition Index (TCI, Table 1). Land surface temperature (LST) can be calculated from the two thermal channels of NOAA–AVHRR by applying different variants of split window algorithms (Price, 1984; Qin & Karnieli, 1999). However, there is a debate how a thermal data set is influenced by a variety of factors including day-of-year, time-of-day and the specific meteorological conditions at the specific-time of image acquisition. McVicar and Jupp (1999, 2002) modeled surface temperatures (as Normalized Difference Temperature Index) taking into account the above factors. They also reported how standard daily meteorological data (either integrals or extremes) can be downscaled to meteorological data at the specific time-of-day, when the thermal remotely sensed data are acquired, as anomaly analysis based on growing season integrals (McVicar & Van Niel, 2005).

Later Kogan (1995, 1997, 2000) developed another index, the Vegetation Health Index (VH, Table 1), which is an additive combination of VCI and TCI, to monitor vegetation health, moisture, and thermal conditions as well as to determine drought-affected areas. The VCI, TCI, and VH have been used as tools for drought detection and vegetation stress mostly in the context of agricultural productions in different parts of the world (Hayes & Decker, 1998; Liu & Kogan, 1996; Kogan, 1995, 1997, 2000; Kogan et al., 2004; Seiler et al., 1998). McVicar and Bierwirth (2001) validated that the ratio of LST and NDVI (LST/NDVI, Table 1) provides a rapid means to assess drought conditions in cloudy environments. A new index – Drought Severity Index (DSI, Table 1) – was invented in framework of this study and compared to the other drought-indices. The DSI is calculated as subtraction of standardized LST and NDVI for a certain month, based on the normalization approach that was suggested by Bayarjargal et al. (2000) to bring different variables (e.g., NDVI and LST) into a same, comparable, scale in terms of their ranges.

Although a considerable number of drought-indices have been developed and used as a monitoring tool for drought or favorable conditions, no comprehensive study for evaluating the performance of these indices has been conducted. The frequent occurrence of droughts in semi-arid environments justifies the need to evaluate the effectiveness of different drought indices. The indices can be compared among themselves and with meteorological-based drought index such as the Palmer Drought Severity Index (PDSI, Table 1) (Palmer, 1965). PDSI measures the accumulated effect of monthly rainfall deficit relative to the monthly rainfall (National Drought Mitigation Center, 2003). PDSI is based on the supply-and-demand concept of the water balance equation, taking into account precipitation and temperature data, as well as availability of the soil water content (Dai et al., 1998). PDSI has been widely used for a variety of applications related to drought monitoring especially in the United States (Heim, 2002; National Drought Mitigation Center, 2003; Woodhouse & Overpeck, 1998) as well as on a global scale (Dai et al., 1998, 2004). Recently the PDSI has been applied by the Mongolian Institute of Meteorology and Hydrology as a standard drought index.

Consequently, the prime objective of this paper is to compare the spatial occurrences of droughts, detected by remotely sensed drought-indices over the desert-steppe and desert geo-botanical zones of Mongolia. This objective was implemented using the Change Vector Analysis technique applied to the NOAA–AVHRR data set and meteorological-derived drought-indices from 1982 to 1999. In order to enhance the evaluation of drought occurrences, the growing season was divided into several sub-periods. In addition, ground-based observations of drought-affected areas for a Soum level are also incorporated in the comparison.

2. Study area

The research was carried out in the Mongolia's desert and desert-steppe geo-botanical zones (Fig. 1). The area covers more than 40% of the country's 1.5 million km^2. The study area includes the Great Lakes Depression, the Valley of Lakes, the plateau of the eastern Gobi and Gobi-Altai Mountains, and the southern and southwestern parts of the Mongolian Gobi. Low grasses, semi-shrubs, and woody plants are the dominant vegetation of the study area, and peak biomass occurs in late summer (Batima et al., 2000). Within the study area hills, hillocks, rolling heaths, and sand dunes are also found. The continental climate of Mongolia is very harsh with sharply defined seasons, high annual and diurnal fluctuations in air temperature, and low precipitation. The mean annual air temperature is about 4 °C. July is the warmest month with an average temperature of 25 °C and maximum temperatures of 35–45 °C (Natsagdorj, 2000). The total annual precipitation is about 90 mm for the whole study area. About 75–85% of the precipitation falls during the three summer months, from June to August (Shiirevdamba, 1998).

3. Materials and data set preparation

The Pathfinder AVHRR Land (PAL) NDVI and brightness temperatures in channels 4 (10.3–11.3 μm) and 5 (11.5–12.5 μm) were used to calculate the drought-indices (Table 1). This data set was composed of monthly maximum values for vegetation growing season (from April to September) over the period of 1982–1999, reprojected from the Goode's equal-area projection to the Geographical projection with spatial resolution of 0.1 × 0.1° in latitude and longitude. The PAL data set was generated from NOAA satellites 7, 9, 11, and 14 (Agbu & James, 1994) and was obtained from the Goddard Space Flight Center (GSFC) Distributed Active Archive Center (DAAC). Radiometric

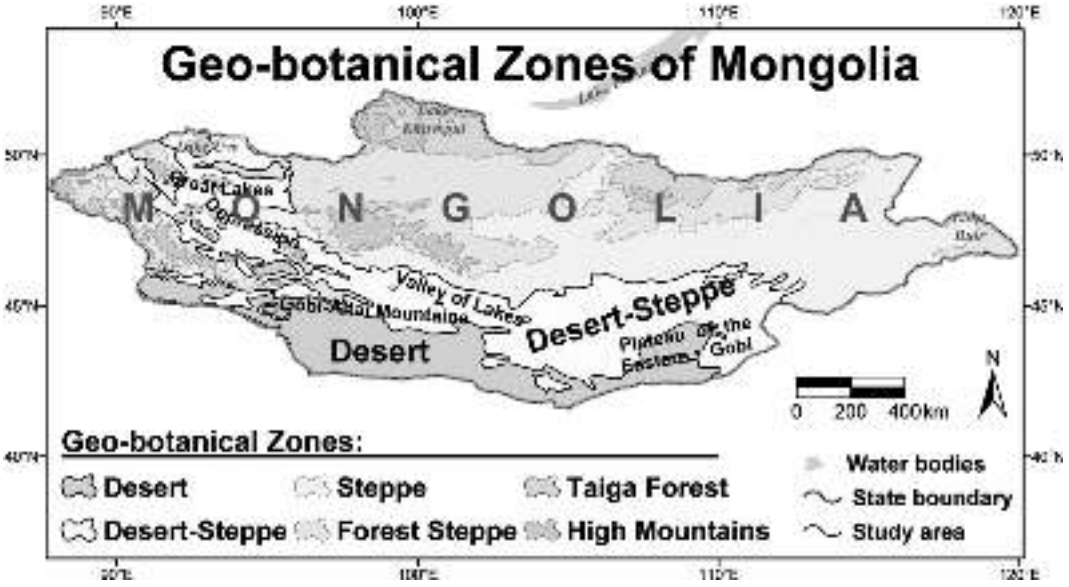

Fig. 1. Study area is restricted to the desert and desert-steppe geo-botanical zones of Mongolia.

calibration, atmospheric correction for Rayleigh scattering, as well as solar zenith angle effects in PAL data set were processed by the Pathfinder processing team (DeFries et al., 2000).

The LST was computed from the brightness temperatures in the thermal channels by a split-window algorithm (Price, 1984) of the form:

$$\mathrm{LST} = T_4 + A(T_4 - T_5) + B(\varepsilon) \tag{1}$$

where T_4 and T_5 are brightness temperatures measured by the AVHRR channels 4 and 5, respectively, $A=2.63$ is a coefficient related to the atmospheric transmittances, being dependent on the atmosphere type, and $B(\varepsilon)=1.27$ is the emissivity effect, which depends on both the channel surface emissivities (ε_4 and ε_5) and atmosphere type. Price (1984) assumed that the emissivity of most of the land surface and vegetation cover is equal to 0.96, thus this value was used in the current research.

The PDSI that was calculated at 56 meteorological stations from 1982 to 1999 for the vegetation growing months (April–September) was obtained from the Meteorological Institute of Mongolia. Monthly PDSI data in a tabular form was spatially interpolated into a raster image format by using spline method of ArcMap (ArcGIS 9.0 version). For interpolation, continues grids of PDSI, with the same Geographical projection and resolution ($0.1\times0.1°$) to the PAL data set were created.

4. Analysis

The eight drought-indices derived from the NOAA–AVHRR and one meteorological-based drought-index (Table 1) are compared for the warm-summer season, since this time is relevant for vegetation monitoring in Mongolia (Tserenjav & Janchivdorj, 1999). Consequently, all data processing in this study was performed for the 6-month vegetation-growing period (VGP) from April to September. Furthermore, the VGP was divided into three sub-parts: the beginning — April and May; the middle — June and July; and the end — August and September.

The change detection technique, CVA, which was adapted to multi-temporal concept by Lambin and Strahler (1994a,b) from the original multi-spectral idea (Malila, 1980; Virag & Colwell, 1987), was used in this study for successive sub-parts of the VGP from 1982 to 1999. Due to its two variables — change magnitude and direction, the CVA has advantage in time-series data compression over other change detection methods.

A pixel value of each drought index, I, for a given year, Y, creates an n-dimensional temporal vector, $\boldsymbol{v}_{I,Y}$, for that given pixel:

$$\boldsymbol{v}_{I,Y} = \begin{bmatrix} I_{t1} \\ I_{t2} \\ \vdots \\ I_{tn} \end{bmatrix} \tag{2}$$

where t is the time dimension, ranges from $t1$ to tn, and n equals to 6 — the relevant VGP months from April to September. Difference between the temporal vectors, $\boldsymbol{v}_{I,Y}$ and the reference year (subscript REF, specified below), is called a temporal change vector, $\boldsymbol{c}_{I,Y}$:

$$\boldsymbol{c}_{I,Y} = \boldsymbol{v}_{I,\mathrm{REF}} - \boldsymbol{v}_{I,Y} \tag{3}$$

The temporal change vector is characterized by a magnitude and direction. The absolute magnitude of the change vector of the index I, $|\boldsymbol{c}_{I,Y}|$, can measure the intensity of the change in vegetation cover caused by drought and is calculated as the Euclidean distance between the index value of the reference and a selected year:

$$|\boldsymbol{c}_{I,Y}| = \sqrt{\sum_{t=1}^{n} (I_{\mathrm{REF}} - I_Y)t^2} \tag{4}$$

The direction of the change vector, $s_{I,Y}$, is measured by the sign between time tn and $tn+1$ caused by subtracting the index value for the reference and selected years for each index I:

$$s_{I,Y} = \pm\left\{(I_{\mathrm{REF}}-I_Y)_{tn+1} \text{ between } (I_{\mathrm{REF}}-I_Y)_{tn}\right\} \quad (5)$$

$s_{I,Y}$ indicates the nature of the change in vegetation cover.

The CVA algorithm was coded into a graphical modeling script within the ERDAS image-processing package (ERDAS, 1997) and applied to the nine different drought indices. The algorithm produces two images for each drought-index, for each year. One image represents the change magnitude (drought intensity) and the other the change direction (drought status). In this research drought status means the onsets or ends of droughts at any sub-part of the vegetation phenology. The change vector directions were coded from 1 to 8 (referred hereinafter as drought categories) according to the sub-parts of the VGP. These categories are: (1) non-drought or favorable condition; (2) drought at the end (August and September); (3) at the middle (June and July); (4) at the middle and end (June to September); (5) at the beginning (April and May); (6) at the beginning and at the end (April and May and August and September); (7) at the beginning and at the middle (April to July) of the VGP; and (8) the entire season of VGP (April to September). It is assumed that a negative value of change vector direction of all the indices between the reference and examined years indicates a decrease of vegetation cover that were caused by the integration of harmful weather variables such as low precipitation and high temperature. Likewise, a positive sign would be assumed for reverse phenomenon. For that reason, it was considered that LST/NDVI and NDVIA would respond to drought when those have positive values in the images of change vector directions, while the other indices would response with negative values. However, direction images of all the drought-indices were coded into same categorical ranges of drought as given above for a comparison purpose.

In the CVA, other two items were considered. One was the concept of a "reference image" that is a reference against which derived change information can be compared (Cohen & Fiorella, 1998). Information of a change can be comparable to a reference, which is a long-term average, median, or minimum profile, and can correspond to the optimum conditions (Lambin & Strahler, 1994b). In the current study, the monthly multi-year medians of the indices were considered as a reference year ($V_{I,\mathrm{REF}}$). The second critical element in CVA was deciding where to place the threshold boundaries between "change" and "non-change" pixels displayed in the histogram of the change image. Thresholds are typically set to a standard deviation value from the mean of the change value histogram of the change image (Lunetta, 1998; Singh, 1989). In this study, one standard deviation above the mean value of change magnitude image's histogram for each index was applied as a threshold boundary for every pixel. Here it was assumed that values above the threshold were resulted due to severe drought conditions.

In order to compare spatial similarity of drought-indices over the growing season, a drought-occurred-area (DOA) map was created for each of nine drought-indices — eight of those were derived from NOAA–AVHRR data set and one was calculated from the meteorological measurement. The DOA map for every index was developed based on a combination of the change direction and magnitude images. Pixel values that were higher than a certain threshold (e.g., one standard deviation above the mean of histogram) in the change magnitude image were sliced and then coded into the drought-categories (Table 2) according to the change direction image. The DOA map for every index indicates occurrences and accumulations of drought events during the VGP for every year in relation to the reference year. The DOA maps of eight satellite-based and one meteorological-derived drought-indices were compared to each other within and between the examined years, and also compared to the traditional drought information observed at the local administration level.

To identify spatial relationships among the drought-indices, pixel-to-pixel paired correlation coefficients were computed between the change magnitude images of the indices for each study year. Since the dynamic ranges of the change vector magnitude images for nine different drought indices are different, a standardization approach was applied to all nine indices before the correlation analysis:

$$|C_{I,Y}|_{standardized} = \frac{|C_{I,Y}|-|C_{I,\Sigma Y}|_{mean}}{|C_{I,\Sigma Y}|_{Stdev}} \quad (6)$$

where $|C_{I,Y}|_{\mathrm{standardized}}$ is the standardized-change-magnitude, with mean value equals to 0 and standard deviation equals to 1, for study year Y for each drought index I, $|\boldsymbol{c}_{I,Y}|$ is the change magnitude value created by Eq. (4), and $|C_{I\sum Y}|_{\mathrm{mean}}$ and $|C_{I\sum Y}|_{\mathrm{Stdev}}$ are the respective multi-year mean and standard deviation. Values that are located above the one standard deviation from the mean of the change magnitude's histogram and would be equal to the

Table 2
Coding drought categories of drought-indices in multi-temporal change vector analysis

Drought category	Direction of change vector of indices in the sub-parts of the VGP			Code description[a]
	Beginning (April and May)	Middle (June and July)	End (August and September)	
1	−	−	−	Favorable condition
				Drought at the:
2	−	−	+	end,
3	−	+	−	middle,
4	−	+	+	middle and end,
5	+	−	−	beginning,
6	+	−	+	beginning and end,
7	+	+	−	beginning and middle
8	+	+	+	entire season of the VGP

Direction of change vectors of drought-indices between the reference and a given years in sub-parts of the VGP.
+ indicates pixel value increase from the one part of the VGP to the next part.
− indicates pixel value decrease from the one part of the VGP to the next part.
[a] The code description is for the drought-indices of NDVI, SVI, VCI, TCI, VH, DSI and PDSI.

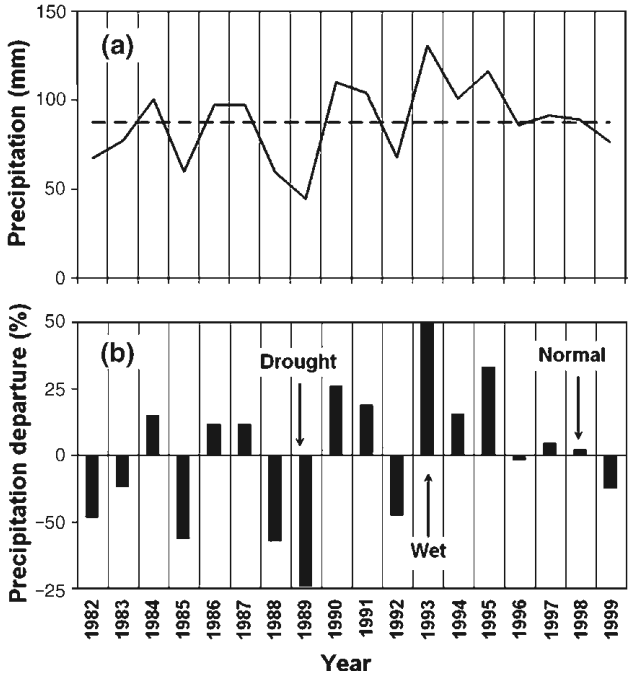

Fig. 2. Annual precipitation (a) and its departure (b) from the normal during the VGP of the study area along the study years (1982–1999). Dashed line in the top chart represents the multi-year mean precipitation.

drought-categories from 2 to 8 were considered in the standardization process (Table 2). When, either the change direction was equal to the drought category 1 (favorable condition in Table 2) or there were no significant changes, no vegetation stress was assumed.

In addition to the spatial comparison of drought-indices, we evaluated drought occurrences at every sub-part of VGP by combining all the satellite-derived indices into a single map. Droughts that were identified by the all indices would be added or overlaid into a combined drought-affected-area (CDOA) map, as every sub-parts of the VGP. Comparison of the combination of satellite-based drought-indices was conducted for the selected years.

5. Results and discussion

Several representative years were selected as a basis for the evaluation of the CVA results, these are: 1993 as a wet year, 1989 as a dry year, and 1998 as a normal year (Fig. 2). For these years, Fig. 3 illustrates drought area identified by different drought-indices disregards to the sub-parts of the VGP. In 1993, the wet year, 3.0–4.6% of the study area is identified as drought by the NDVI and NDVIA, while 0.3–0.8% is identified by the SVI, VCI, and LST/NDVI (Fig. 3a). In this year, the TCI, VH, and DSI detect relatively less areas as drought (0.04–0.2%) while no drought areas are identified by the meteorological-derived drought-index (Fig. 3a). In 1989, the drought year, 15.6–16.4% of the study area is identified as drought by all indices but the LST/NDVI that show lower value (Fig. 3b). In this year 17.4% of the study area is detected as drought by the PDSI (Fig. 3b). Therefore, it should be noted that in this year there is a good agreement among the satellite- and meteorological-derived drought-indices. In 1998, the normal year, 6.6–9.9% of the area is identified as drought by the reflective indices (Fig. 3c). Also, 9.1% of the study area is marked as drought by the LST/NDVI. These findings are similar to the meteorological-based PDSI, which marked 10.5% of the study area as affected by drought. The thermal index and hybrid indices show that larger areas, 12–16.9% of the total study area, are affected by drought in this year.

The DOA maps, resulted from the CVA, for the nine satellite- and meteorological-derived drought-indices are shown in Figs. 4 5 and 6. The drought categories are compatible with Table 2. The DOA maps of drought-indices are evaluated against the traditional drought-affected-area (DAA) maps for wet (1993) and drought (1989) years (Figs. 4j and 5j), except for the normal year (1998) due to lacked ground data. The DAA maps were created from the tabular data within the local administration boundary. Therefore, it should be noted that the traditional method DAA map does not distinguish between sub-parts of the VGP, as can be analyzed with the image- and meteorological-derived drought-indices.

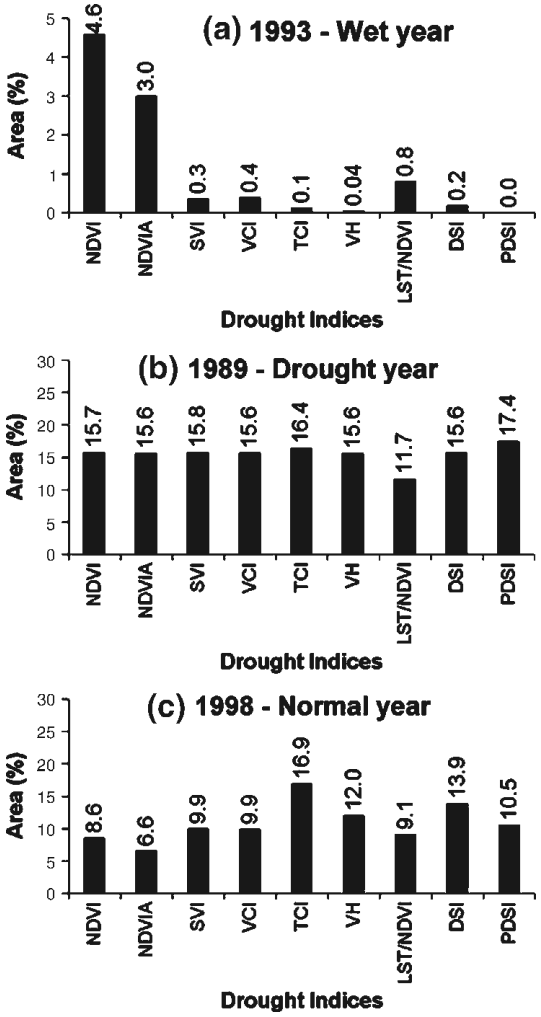

Fig. 3. The total drought area identified by the different drought-indices by all drought categories occurred in sub-parts of the VGP, for each of eight different remotely sensed drought-indices and one meteorological drought-index in (a) wet, (b) drought, and (c) normal years.

Fig. 4 illustrates the wet year DOA maps for drought-indices. It can be noticed that the reflective indices (Fig. 4a–d) identify relatively small areas as drought at the beginning (spring) of the growing season (category 5, Table 2) in the Great Lakes Depression and in the fringe of the Eastern Gobi Plateau, which are large sandy areas. Only a few pixels were detected as drought by LST/NDVI in the southern-fringe and central parts of the Gobi Desert, (Fig. 4g). Also, TCI and DSI were found small drought areas in the south center of study area (Fig. 4e,h). The PDSI did not show any indication of drought (Fig. 4i), while the DAA map marks much larger areas as drought for this year (Fig. 4j). This ground observation does not match with the reflective indices and partly matches to the LST/NDVI area.

In 1989, when precipitation was significantly below normal (Fig. 2), droughts occurred over relatively large areas as shown by the DOA maps of the satellite- and meteorological-derived drought-indices (Fig. 5a–i) as well as in the DAA map (Fig. 5j). For this dry year, most droughts are identified as combinations of drought categories of the VGP (rather than a single category) by the reflective indices. The Depression of Great Lakes, the Valley of Lakes, bottom of the Gobi-Altai Mountains, and the Plateau of Eastern Gobi are identified as droughts occurred from the middle to the late of the VGP (i.e., summer–autumn drought that is a category 4, Table 2) or entirely occurred drought (category 8) by these indices (Fig. 5a,b,c,d). The reflective indices exhibit almost similar results. The Valley of Lakes, lower parts of the Great Lakes Depression, the Gobi-Altai Mountain, south of the Plateau of Eastern Gobi and Gobi Desert areas in the southwest of the study area are identified as entirely occurred droughts by the thermal index (Fig. 5e), and the hybrid indices (Fig. 5f,g,h).

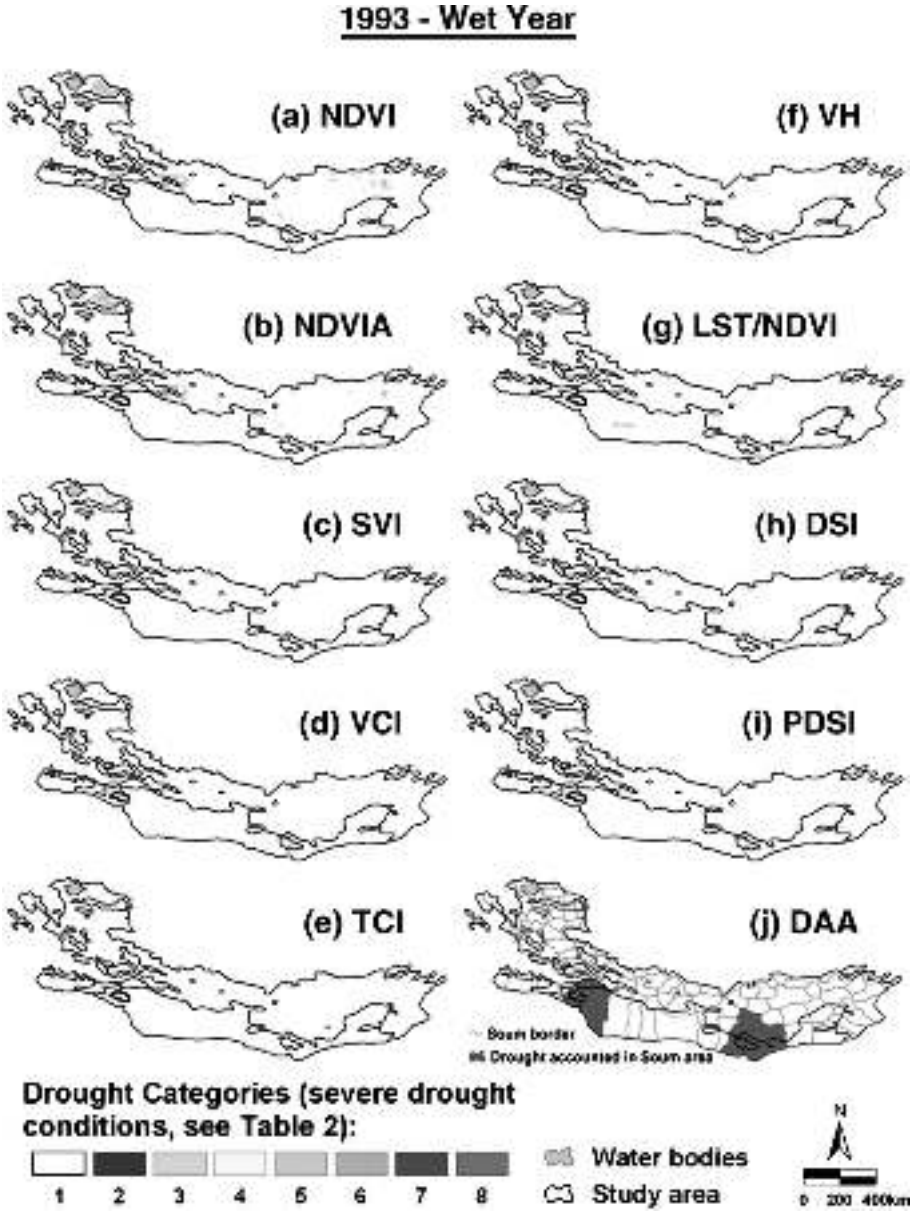

Fig. 4. Comparison of CVA based DOA maps of satellite- and meteorological-derived drought-indices over sub-parts of the VGP for 1993 in desert and desert-steppe geo-botanical zones of Mongolia. Ground observed DAA are also shown. Indices are according to Table 1 and drought categories are according to Table 2.

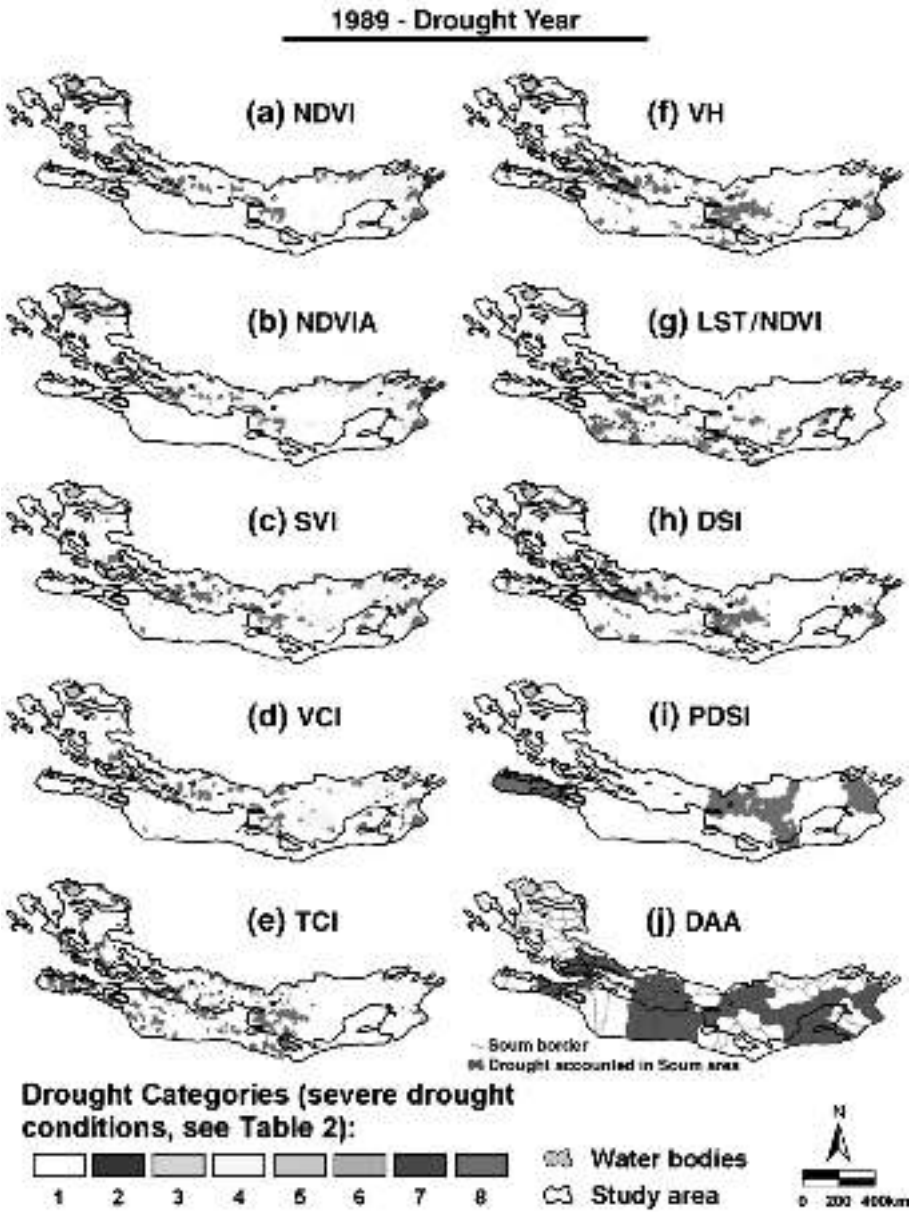

Fig. 5. Same as Fig. 3, but for 1989 (dry year).

These hybrid indices have similar meaning. In addition, the LST/NDVI detects droughts in the middle (summer), end (autumn), and entire period of the VGP. The DOA maps of remotely sensed drought indices only partially match the PDSI map that shows three drought-affected areas (Fig. 5i). The western one partially matches only to the TCI, the central area matches to the VH and DSI, and the eastern area partially matches to the reflective indices. Entire-season droughts (i.e., drought category 8) are found by the PDSI in the Plateau of Eastern Gobi and the western point of the study area. More surprising is the DAA map that almost systematically marks larger areas than the satellite- and meteorological-derived indices (Fig. 5j). The reason can be explained by the different sources of information used for the drought-indices and DAA map. Drought indices were developed from the spatially continuing data sets. On the other hand, DAA map was created from tabular data where drought occurrences were marked over the whole area of a local administration. Since the boundary and timely information of the ground based DAA was not clear (e.g., where and how large area of the Soum territory was affected by drought) it was not sufficient to compare with remotely sensed drought indices.

Small areas in the Depression of Great Lakes in the northwestern fringe, in the Plateau of Eastern Gobi, and in the eastern and central parts of the study area are identified as droughts at different sub-parts of the VGP in 1998 (normal year) by the DOA maps of the reflective indices (Fig. 6a,b,c,d). Early droughts continued to the middle (summer) of the VGP (drought categories of 3, 5, and 7, Table 2) are found in these areas. Dissimilarly, relatively larger areas over the Gobi Desert in the south-central parts of the study area are identified as drought over the beginning–middle (category 7), the middle–end (category 4), and entirely season (category 8) of the VGP in

the DOA of the thermal and hybrid indices as well as in the DSI map (Fig. 6e,f,g,h). Larger area in the Plateau of Eastern Gobi in the east of the study area shows similar drought patterns on the DOA maps of the satellite derived indices and the PDSI in sub-parts of the VGP in the year with normal precipitation. Beginning and beginning–middle (i.e., summer and summer–autumn) droughts in the Plateau of Eastern Gobi and entirely occurred droughts are found by the PDSI in the north of the Great Lakes Depression and west point of the Gobi (Fig. 6i). Consequently, the PDSI partially match to different groups of drought-spectral indices derived in this year.

The pixel-to-pixel paired correlation was applied to the standardized change-magnitude images for eight satellite based and one meteorological-derived drought-indices. Correlation matrix (r) among the indices is presented in Table 3, for selected years with different rainfall regimes and for the average of 18-year period from 1982 to 1999. In the wet year Table 3a reveals relatively poor but mostly significant correlations among the indices except for the NDVI and NDVIA, which are positively related. In the normal and dry years and also in the multi-year average, significant high correlations are found among the reflective indices (Table 3b,c,d). All other correlations, among

Table 3
Correlation matrix (r) among the satellite- and meteorological-derived drought-indices for the years with different rainfall conditions: (a) wet year (1993), (b) dry year (1989), (c) normal year (1998), and (d) 18-year average

Drought indices (# of pixels)	NDVI (4214)	NDVIA (4189)	SVI (7110)	VCI (7406)	TCI (6964)	VH (3313)	LST/NDVI (7365)	DSI (7365)	PDSI (5803)
(a) 1993 (wet year)									
NDVI	1								
NDVIA	**0.75**	1							
SVI	*0.24*	*0.28*	1						
VCI	*0.29*	*0.29*	*0.49*	1					
TCI	0.00	0.00	0.02	*0.03*	1				
VH	*0.15*	*0.15*	*0.16*	*0.22*	*0.17*	1			
LST/NDVI	*−0.10*	*−0.14*	*−0.07*	*−0.10*	*−0.14*	*−0.32*	1		
DSI	*0.10*	0.10	*0.11*	*0.17*	*0.12*	*0.38*	*−0.09*	1	
PDSI	*−0.03*	*−0.02*	*0.03*	*0.02*	*0.03*	*−0.07*	*−0.19*	*−0.02*	1
(b) 1989 (dry year)									
NDVI	1								
NDVIA	**0.84**	1							
SVI	**0.57**	**0.59**	1						
VCI	**0.59**	**0.58**	**0.80**	1					
TCI	*0.04*	*0.04*	*0.06*	*0.07*	1				
VH	*0.35*	*0.34*	*0.44*	*0.44*	*0.38*	1			
LST/NDVI	*0.10*	*0.10*	*0.23*	*0.20*	*0.07*	*0.24*	1		
DSI	*0.34*	0.32	*0.41*	*0.40*	*0.38*	**0.78**	*0.23*	1	
PDSI	*0.10*	0.11	*0.14*	*0.11*	*0.01*	*0.05*	0.00	*0.04*	1
(c) 1998 (normal year)									
NDVI	1								
NDVIA	**0.86**	1							
SVI	**0.68**	**0.66**	1						
VCI	**0.71**	**0.67**	0.84	1					
TCI	*−0.04*	*−0.03*	0.01	0.01	1				
VH	*0.22*	*0.21*	0.30	0.31	0.36	1			
LST/NDVI	*0.03*	*0.03*	0.04	0.05	0.04	0.19	1		
DSI	*0.20*	0.20	*0.26*	*0.26*	*0.37*	**0.67**	*0.24*	1	
PDSI	*0.14*	0.11	*0.17*	*0.18*	*0.08*	*0.22*	*0.15*	*0.24*	1
(d) Multi-year average (1982–1999)									
NDVI	1								
NDVIA	**0.83**	1							
SVI	**0.58**	**0.56**	1						
VCI	**0.63**	**0.58**	**0.82**	1					
TCI	0.08	0.07	0.08	0.08	1				
VH	*0.38*	*0.35*	*0.40*	*0.41*	*0.35*	1			
LST/NDVI	*0.27*	*0.25*	*0.37*	*0.33*	*0.11*	*0.33*	1		
DSI	*0.40*	0.36	*0.44*	*0.43*	*0.33*	**0.69**	*0.36*	1	
PDSI	*0.06*	0.06	*0.13*	*0.11*	*0.13*	*0.09*	*0.06*	*0.13*	1

The number of pixels that is used for the correlation analysis for every index is shown in parentheses. These numbers are different for each index, since a favorable condition (e.g., drought category # 1 in Table 2) is excluded in the correlation analysis. Higher correlations are marked in bold and significant values at the $p<0.05$ are shown as italics.

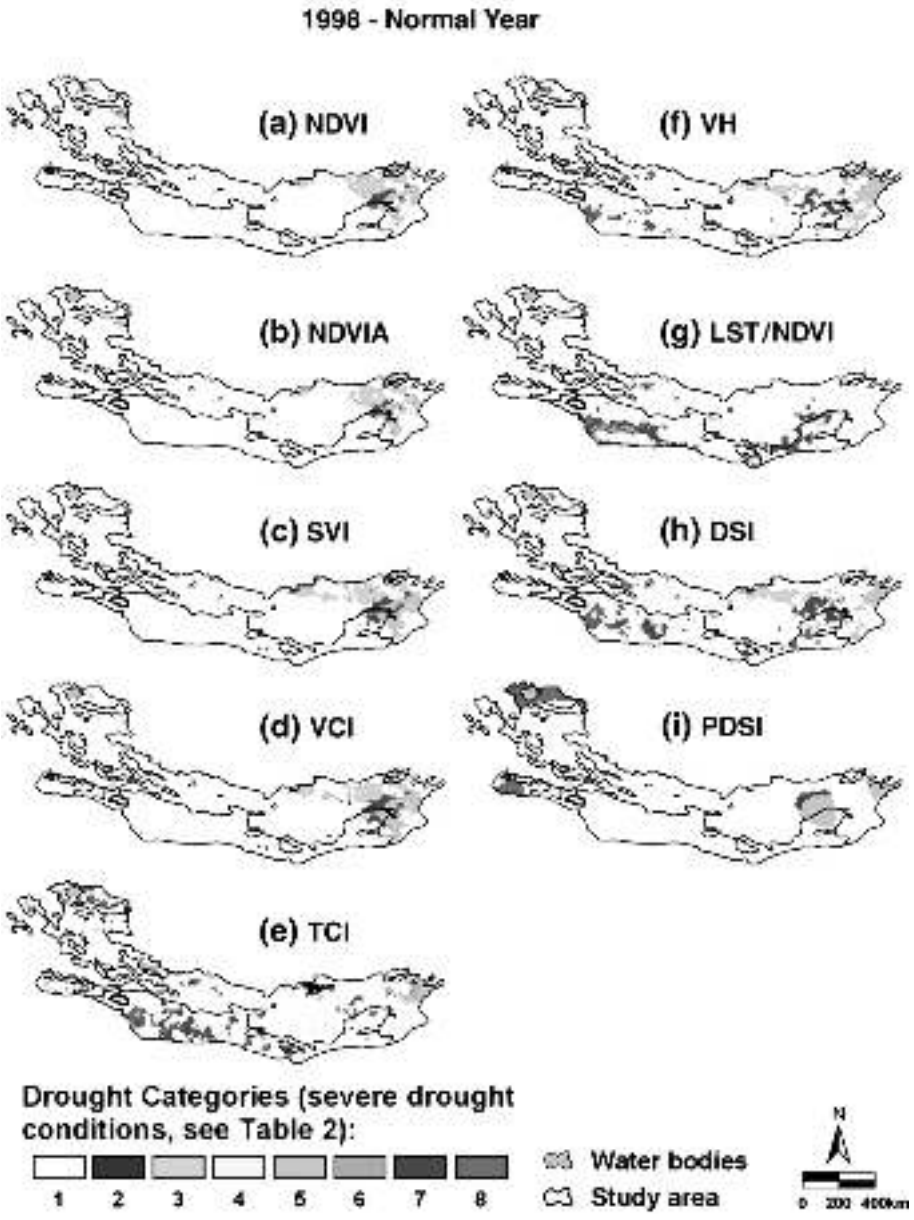

Fig. 6. Same as Fig. 3, but for 1998 (normal year). Due to lack of ground data, the DAA map is not shown.

the thermal and hybrid indices as well as among these indices and the reflective ones are rather poor, under all precipitation regimes, except for the correlation between DSI and VH for drought and normal years, as well as for multi-year average. All correlations between the satellite-derived indices and the PDSI were also found to be very poor.

The combined drought-affected-area (CDOA) maps of the satellite-derived drought indices in different drought categories for selected wet, dry, and normal years are displayed in Fig. 7. The CDOA map can be interpreted by drought categories and code descriptions with Table 2. The CDOA maps show that there are mostly short-term drought events in the wet year, 1993, such as drought at the beginning, middle, and end of the VGP (Fig. 7a and drought categories of 5, 3, and 2 in Table 2). However, in the dry year (1989), most droughts are detected at the middle, middle and end, and along the entire season of VGP (Fig. 7b and drought categories 8, 4, and 2). Natsagdorj (2000) noted that if drought in Mongolia starts at the beginning of growing season it mostly continued over year round. However, droughts at the beginning of the growing season would be more difficult to interpret as air temperature could still be low resulting in decreased growth. In 1998 (the year with normal rainfall), in addition to the short-term droughts during early, middle, and late sub-parts of the VGP (Fig. 7c and drought categories 5, 3, and 2), longer droughts over two or more sub-parts of the VGP happened (drought categories 7, 6, and 4). Generally, relatively larger areas are identified as droughts in sub-parts of the VGP when all drought categories are overlaid onto a single map — CDOA map, although rainfall was around normal (Fig. 7c). Also, as expected, larger areas are detected as drought over the whole VGP in the study area by the summation of all drought categories of satellite indices in drought year (Fig. 7b). By

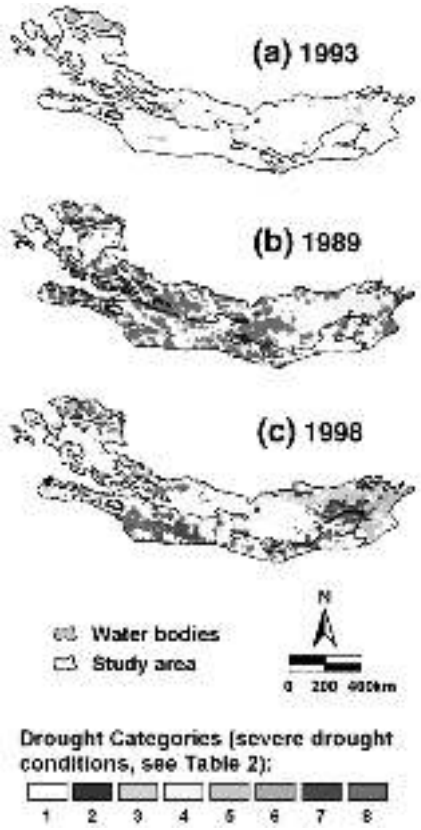

Fig. 7. Comparison of the CDOA maps of all drought indices are overlaid into a single map with drought categories at the sub-part of the VGP for 1993 year with higher than normal precipitation (a), for 1989 drought year (b), and for 1998 with normal precipitation (c).

summing all drought categories of all drought-indices, the drought area is much larger than the areas either in PDSI map (Figs. 4i, 5i and 6i) or traditional DAA maps (Figs. 4j and 5j). This might be explained by differences of observation and calculation methods between the remote sensing and meteorological measurements, although various normalization or/and interpolation approaches have been applied to those data set (e.g., a maximum value composite technique for AVHRR data set (Holben, 1986); calculate then interpolate method (McVicar & Jupp, 2002) for meteorological PDSI). Also, precision of ground measured DAA maps at the local level might not be enough to compare to the remote sensing indices.

6. Conclusions

Remote sensing Change Vector Analysis was used to compare the spatial distributions of drought-detection indices derived from the reflective and thermal channels of the NOAA–AVHRR sensor over the desert and desert-steppe geo-botanical zones of Mongolia. It can be concluded that:

- There are good agreements among the different satellite-derived drought indices and also between these and the meteorological-derived drought-index in terms of estimation of the entire affected area in dry year.
- There is no consistent spatial overlapping among the satellite-derived drought indices. Different groups of indices identify different areas as drought in different parts of the vegetation growing period and under different precipitation regimes. Reflective indices, such as NDVI or NDVI-derived NDVIA, SVI and VCI, due to their formulation, produce almost similar results. Similarities were found between the thermal index, TCI, and among the hybrid indices such as VH, LST/NDVI and DSI. This finding raises a question about the reliability of vegetation indices to assess droughts.
- There are partial agreements between the meteorological drought index PDSI and the different groups of the satellite-derived drought indices.
- There is no agreement between the traditional ground-observed drought-affected-areas maps and the satellite-derived drought indices. Wider areas are identified as droughts by overlaying all the satellite-derived drought indices than by the ground-observation map. This can reveal that the precision of meteorological measurements and ground observations at the local level is not sufficient to compare remotely sensed drought indices over wide regions.
- Statistical results show that relatively higher correlations were found among the reflective indices than among the thermal and the hybrid ones. Poor correlations are found between the satellite- and meteorological-derived drought-indices.
- Finally, the differences in the ability of the eight different drought indices to detect the drought occurrences and status with respect to ground-observations emphasize the importance to study the evaluation performances of the indices for further utilization of this information.

Acknowledgement

This project was partially supported by the EU-INCO program (Grant No. ICA2 CT 2000 10022) and partially by the USAID-CDR (Grant No. TA-MOU-00-C20-010).

References

Adyasuren, T. (1998). State of drought and desertification in Mongolia. In B. Darin (Ed.), *Environment and development issues in Mongolia* (pp. 96). Ulaanbaatar, Mongolia: InterPress.

Agbu, P. A., & James, M. E. (1994). The NOAA/NASA pathfinder AVHRR land data set user's manual. *Goddard distributed active archive center, NASA* Greenbelt: Goddard Space Flight Center.

Anyamba, A., Tucker, C. J., & Eastman, J. R. (2001). NDVI anomaly patterns over Africa during the 1997/98 ENSO warm event. *International Journal of Remote Sensing*, *22*, 1847−1859.

Batima, P., Bolortsetseg, B., Mijjiddorj, R., Tumerbaatar, D., & Ulziisaihan, V. (2000). Impacts on natural resource base. In P. Batima & D. Dagvadorj (Eds.), *Climate change its impacts in Mongolia* (pp. 47−96). Mongolia: JEMR.

Bayarjargal, Y., Adyasuren, T., & Munkhtuya, S. (2000). Drought and vegetation monitoring in the arid and semi-arid regions of the Mongolia using remote sensing and ground data. *Proceedings of 21st Asian Conference on Remote Sensing, Taipei, Taiwan*, *Vol. 1*. (pp. 372−377) Available online at http://www.gisdevelopment.net/aars/acrs/2000/ts8/index.shtml

Bolortsetseg, B., Bayasgalan, Sh., Dorj, B., Natsagdorj, L., & Tuvaansuren, G. (2000). Impacts on agriculture. In P. Batima & D. Dagvadorj (Eds.), *Climate change its impacts in Mongolia* (pp. 97−199). Mongolia: JEMR.

Cohen, W., & Fiorella, M. (1998). Comparison of methods for detecting conifer forest change with thematic mapper imagery. In R. S. Lunetta & C. D. Elvidge (Eds.), *Remote sensing change detection: Environmental monitoring methods and applications* (pp. 89−102). Michigan, USA: Ann Arbor Press.

Collins, J. B., & Woodcock, C. E. (1996). An assessment of several linear change detection techniques for mapping forest mortality using multitemporal Landsat TM data. *Remote Sensing of Environment*, *56*, 66−77.

Dai, A., Trenberth, K. E., & Karl, T. R. (1998). Global variations in droughts and wet spells: 1900–1995. *Geophysical Research Letters*, *25*, 3367−3370.

Dai, A., Trenberth, K. E., & Qian, T. (2004). A global data set of Palmer Drought Severity Index for 1870–2002: Relationship with soil moisture and effects of surface warming. *Journal of Hydrometeorology*, *5*, 1117−1130.

DeFries, R. S., Hansen, M. C., & Townshend, J. R. G. (2000). Global continuation fields of vegetation characteristics: A linear mixture model applied to multi-year AVHRR data. *International Journal of Remote Sensing*, *21*, 1389−1414.

Diouf, A., & Lambin, E. F. (2001). Monitoring land-cover changes in semi-arid regions: Remote sensing data and field observations in the Ferlo, Senegal. *Journal of Arid Environments*, *48*, 129−148.

ERDAS (1997). *ERDAS field guide* (pp. 655). Atlanta: ERDAS Inc.

Gonzalez-Alonso, F., Calle, A., Casanova, J. L., Vazquez, A., & Cuevas, J. M. (2000). Operational monitoring of drought in Spain using NOAA–AVHRR satellite images. *Proceedings of 28th International Symposium on Remote Sensing of Environment, 27–31 March, Cape Town, South Africa*.

Gonzalez-Alonso, F., Cuevas, J. M., Casanova, J. L., Calle, A., & Illera, P. (1995). Drought monitoring in Spain using satellite remote sensing. In Askne (Ed.), *Sensors and environmental applications of remote sensing* (pp. 87−90). Rotterdam: Balkema.

Gutman, G. (1990). Towards monitoring droughts from space. *Journal of Climate*, *3*, 282−295.

Hayes, M. J., & Decker, W. L. (1998). Using satellite and real-time weather data to predict maize production. *International Journal of Biometeorology*, *42*, 10−15.

Heim, R. R. (2002). A review of twentieth-century drought indices used in the United States. *Bulletin of the American Meteorological Society*, *84*, 1149−1165.

Hielkema, J. U., Prince, S. D., & Astle, W. L. (1986). Rainfall and vegetation monitoring in the Savanna Zone of Sudan using the NOAA AVHRR data. *International Journal of Remote Sensing*, *7*, 1499−1513.

Holben, B. N. (1986). Characteristics of maximum-value composite images from temporal AVHRR data. *International Journal of Remote Sensing*, *7*, 1417−1434.

Huete, A. R., & Tucker, C. J. (1991). Investigation of soil influences on AVHRR red and near-infrared vegetation index imagery. *International Journal of Remote Sensing*, *12*, 1223−1242.

Hulme, M., & Kelly, M. (1993). Exploring the links between desertification and climate change. *Environment*, *35*, 4−11.

Ji, L., & Peters, A. (2003). Assessing vegetation response to drought in the northern Great Plains using vegetation and drought indices. *Remote Sensing of Environment*, *87*, 85−98.

Johnson, R. D., & Kasischke, E. S. (1998). Change vector analysis: A technique for the multispectral monitoring of land cover and condition. *International Journal of Remote Sensing*, *19*, 411−426.

Karnieli, A. (2000). Drought monitoring in the Negev Desert using NOAA/AVHRR Imagery. *Proceedings of "Agroenviron-2000" 2nd International Symposium on New Technologies for Environmental Monitoring and Agro-Applications, 18–20 October, Tekirdag* (pp. 77−82). Turkey: Trajya-University Printing Press.

Karnieli, A., Bayasgalan, M., Bayarjargal, Y., Khudulmur, S. & Tucker C. J. (in press). Comments on the use of the Vegetation Health Index over Mongolia. *International Journal of Remote Sensing*.

Karnieli, A., & Dall'Olmo, G. (2003). Remote sensing monitoring of desertification, phenology, and droughts. *Management of Environmental Quality: An International Journal*, *14*, 22−38.

Karnieli, A., Shachak, M., Tsoar, H., Zaady, E., Kaufman, Y., Danin, A., et al. (1996). The effect of microphytes on the spectral reflectance of vegetation in semi-arid regions. *Remote Sensing of Environment*, *57*, 88−96.

Kauth, R. J., & Thomas, G. S. (1976). The tessled cap—a graphic description of the spectral–temporal development of agricultural crops as seen by Landsat. *Proceedings of the Symposium on Machine Processing of Remotely Sensed Data* (pp. 4B41−4B51). West Lafayette, Indiana, USA: Purdue University.

Kogan, F. N. (1990). Remote sensing of weather impacts on vegetation in non-homogeneous areas. *International Journal of Remote Sensing*, *11*, 1405−1419.

Kogan, F. N. (1995). Application of vegetation index and brightness temperature for drought detection. *Advances in Space Research*, *11*, 91−100.

Kogan, F. N. (1997). Global drought watch from space. *Bulletin of the American Meteorological Society*, *78*, 621−636.

Kogan, F. N. (2000). Contribution of remote sensing to drought early warning. In D. A. Wilhite, M. V. K. Sivakumar, & D. A. Wood (Eds.), *Early warning systems for drought preparedness and drought management: Proceedings of an Expert Group Meeting, 5–7 September, Lisbon, Portugal* (pp. 86−100). Geneva, Switzerland: WMO.

Kogan, F. N., Usa, D. C., Stark, R., Gitelson, A., Jargalsaikhan, L., Dugarjav, C., et al. (2004). Derivation of pasture biomass in Mongolia from AVHRR-based vegetation health indices. *International Journal of Remote Sensing*, *25*, 2889−2896.

Lambin, E. F., & Strahler, A. H. (1994). Indicators of land cover change for change vector analysis in multitemporal space at coarse spatial scales. *International Journal of Remote Sensing*, *10*, 2099−2119.

Lambin, E. F., & Strahler, A. H. (1994). Change-vector analysis in multitemporal space: A tool to detect and categorize land-cover change processes using high temporal-resolution satellite data. *Remote Sensing of Environment*, *48*, 231−244.

Lambin, E. F., & Ehrlich, D. (1996). The surface temperature–vegetation index space for land cover and land-cover change analysis. *International Journal of Remote Sensing*, *17*, 463−478.

Lambin, E. F., & Ehrlich, D. (1997). Land-cover changes in Sub-Saharan Africa (1982–1991): Application of a change index based on remotely sensed surface temperature and vegetation indices at a continental scale. *Remote Sensing of Environment*, *61*, 181−200.

Liu, W. T., & Kogan, F. N. (1996). Monitoring regional drought using the vegetation condition index. *International Journal of Remote Sensing*, *17*, 2761−2782.

Liu, W. T., & Negron-Juarez, R. I. (2001). ENSO drought onset prediction in northeast Brazil using NDVI. *International Journal of Remote Sensing*, *22*, 3483−3501.

Lunetta, R. S. (1998). Project formulation and analysis approaches. In R. S. Lunetta & C. D. Elvidge (Eds.), *Remote sensing change detection: Environmental monitoring methods and applications* (pp. 1−19). Michigan, USA: Ann Arbor Press.

Lunetta, R. S., & Elvidge, C. D. (1998). *Remote sensing change detection: Environmental monitoring methods and applications* (pp. 318). Michigan, USA: Ann Arbor Press.

Malila, W. A. (1980). Change vector analysis: An approach for detecting forest changes with Landsat. Proceedings Sixth Annual Symposium Machine Processing of Remotely Sensed Data. In P. G. Burroff & D.B. Morrison (Eds.), *Soil information systems and remote sensing and soil survey* (pp. 326−335). West Lafayette, IN: Purdue U. Lab. App. Remote Sens 3–6 June.

Malingreau, J. -P. (1986). Global vegetation dynamics: Satellite observations over Asia. *International Journal of Remote Sensing*, *9*, 1121−1146.

Maselli, F., Conese, C., Petkov, L., & Gilabert, M. A. (1993). Environmental monitoring and crop forecasting in the Sahel through the use of NOAA NDVI data. A case study: Niger 1986–89. *International Journal of Remote Sensing*, *14*, 3471−3487.

McCarthy, J. J., Canziani, O. F., Leary, N. A., Dokken, D. J., & White, K. S. (2001). Climate change 2001: Impacts. *Adaptation and vulnerability* (pp. 1000). UK: Cambridge University Press.

McVicar, T. R., & Bierwirth, P. N. (2001). Rapidly assessing the 1997 drought in Papua New Guinea using composite AVHRR imagery. *International Journal of Remote Sensing*, *22*, 2109−2128.

McVicar, T. R., & Jupp, D. L. B. (1998). The current and potential operational uses of remote sensing to aid decisions on drought exceptional circumstances in Australia: A review. *Agricultural Systems*, *57*, 399−468.

McVicar, T. R., & Jupp, D. L. B. (1999). Estimating one-time-of-day meteorological data from standard daily data as inputs to thermal remote

sensing based energy balance models. *Agriculture and Forest Meteorology*, *96*, 219−238.

McVicar, T. R., & Jupp, D. L. B. (2002). Using covariates to spatially interpolate moisture availability in the Murray-Darling Basin: A novel use of remotely sensed data. *Remote Sensing of Environment*, *79*, 199−212.

McVicar, T. R., & Van Niel, T. G. (2005). Deriving moisture availability from time series remote sensing for drought assessment. *Report to the Reference Group of the Australian Water Availability Project (AWAP). CSIRO Land and Water Client Report, Canberra, Australia* (pp. 29). http://www.clw.csiro.au/publications/consultancy/2005/deriving_moisture_availability_AWAP.pdf

National Drought Mitigation Center (2003). What is drought? Drought indices. http://www.drought.unl.edu/whatis/indices.htm

Natsagdorj, L. (2000). Climate change. In P. Batima, & D. Dagvadorj (Eds.), *Climate change its impacts in Mongolia* (pp. 15−42). Mongolia: JEMR.

Nemani, R. R., & Running, S. W. (1989). Estimation of regional surface resistance to evapotranspiration from NDVI and thermal-IR AVHRR data. *Journal of Applied Meteorology*, *28*, 276−284.

Nicholson, S. E., & Farrar, T. J. (1994). The influence of soil type on the relationships between NDVI, rainfall, and soil moisture in semiarid Botswana: I. NDVI response to rainfall. *Remote Sensing of Environment*, *50*, 107−120.

Nicholson, S. E., Tucker, C. J., & Ba, M. B. (1998). Desertification, drought and surface vegetation: An example from the West African Sahel. *Bulletin of the American Meteorological Society*, *79*, 815−829.

Palmer, W. C. (1965). *Meteorological drought. Research Paper vol. 45* Washington, DC: US Weather Bureau.

Peters, A. J., & Eve, M. D. (1995). Satellite monitoring of desert plant community response to moisture availability. *Environmental Monitoring and Assessment*, *37*, 273−287.

Peters, A. J., Reed, B. C., Eva, M. D., & Havstad, K. M. (1993). Satellite assessment of drought impact on native plant communities of southeastern New Mexico, U.S.A. *Journal of Arid Environments*, *24*, 305−319.

Peters, A. J., Walter-Shea, E. A., Ji, L., Vina, A., Hayes, M., & Svoboda, M. D. (2002). Drought monitoring with NDVI-based standardized vegetation index. *Photogrammetric Engineering and Remote Sensing*, *68*, 71−75.

Price, J. C. (1984). Land surface temperature measurements from the split window channels of the NOAA 7 advanced very high resolution radiometer. *Journal of Geophysical Research*, *89*, 7231−7237.

Prince, S. D., De Colstoun, E. B., & Kravitz, L. L. (1998). Evidence from rain-use efficiencies does not indicate extensive Sahelian desertification. *Global Change Biology*, *4*, 359−374.

Qin, Z., & Karnieli, A. (1999). Progress in the remote sensing of land surface temperature and ground emissivity using NOAA–AVHRR. *International Journal of Remote Sensing*, *20*, 2367−2393.

Richard, Y., & Poccard, I. (1998). A statistical study of NDVI sensitivity to seasonal and interannual rainfall variations in southern Africa. *International Journal of Remote Sensing*, *19*, 2907−2920.

Salinas-Zavala, C. A., Douglas, A. V., & Diaz, H. F. (2002). Interannual variability of NDVI in northwest Mexico. Associated climatic mechanisms and ecological implications. *Remote Sensing of Environment*, *82*, 417−430.

Schmidt, H., & Karnieli, A. (2000). Remote sensing of the seasonal variability of vegetation in a semi-arid environment. *Journal of Arid Environments*, *45*, 43−59.

Seiler, R. A., Kogan, F., & Sullivan, J. (1998). AVHRR-based vegetation and temperature condition indices for drought detection in Argentina. *Advances in Space Research*, *21*, 481−484.

Shiirevdamba, T. (1998). Biological diversity in Mongolia: First national report. *Ministry for nature and the environment of Mongolia* (pp. 106). Ulaanbaatar, Mongolia: Admon printing house.

Singh, A. (1989). Digital change detection techniques using remotely sensed data. *International Journal of Remote Sensing*, *10*, 989–100.

Srivastava, S. K., Jayaraman, V., Rao, P. P. N., Manikiam, B., & Chandrasekhar, M. G. (1997). Interlinkages of NOAA/AVHRR derived integrated NDVI to seasonal precipitation and transpiration in dryland tropics. *International Journal of Remote Sensing*, *18*, 2931−2952.

Tserenjav, G., & Janchivdorj, L. (1999). Water supply problems in the Gobi-desert zone and desertification criteria. In T. Adyasuren (Ed.), *Some aspects to combat desertification in Mongolia* (pp. 52−60). Ulaanbaatar, Mongolia: InterPress (in Mongolian).

Tucker, C. J. (1979). Red and photographic infrared linear combinations for monitoring vegetation. *Remote Sensing of Environment*, *8*, 127−150.

Tucker, C. J. (1989). Comparing SMMR and AVHRR data for drought monitoring. *International Journal of Remote Sensing*, *10*, 1663−1672.

Tucker, C. J., & Choudhury, B. J. (1987). Satellite remote sensing of drought conditions. *Remote Sensing of Environment*, *23*, 243−251.

Tucker, C. J., Vanpraet, C., Sharman, M. J., & Van Ittersum, G. (1985). Satellite remote sensing of total herbaceous biomass production in the Senegalese Sahel: 1980–1984. *Remote Sensing of Environment*, *17*, 233−249.

Virag, L. A., & Colwell, J. E. (1987). An improved procedure for analysis of change in Thematic Mapper image-pairs. *Proceedings of 21st International Symposium on Remote Sensing of Environment* (pp. 1101−1110). Michigan, USA: Ann Arbor Press.

Woodhouse, C. A., & Overpeck, J. T. (1998). 2000 years of drought variability in the central United States. *Bulletin of the American Meteorological Society*, *79*, 2693−2714.